IL NUOVO CIMENTO **40 C** (2017) 84
DOI 10.1393/ncc/i2017-17084-7

COMMUNICATIONS: SIF Congress 2016

Study of quadrupole correlations in the neutron-deficient Sn and Cd region via lifetime measurements

M. SICILIANO([1])([2])

([1]) *Dipartimento di Fisica e Astronomia, Università di Padova - Padova, Italy*
([2]) *INFN, Laboratori Nazionali di Legnaro - Legnaro, Italy*

received 15 February 2017

Summary. — During the AGATA campaign at GANIL (France), the neutron-deficient Sn region was populated via a multi-nucleon transfer reaction in order to directly measure the lifetime of the first excited states with a plunger device to study the evolution of the shell closure in the vicinity of ^{100}Sn. The AGATA γ-ray array was used together with the VAMOS++ spectrometer to study the nuclei of interest. In this contribution the first results confirming the validity of the method for ^{106}Cd and the setup will be presented.

1. – Introduction

The last decade has witnessed both quantitative and qualitative progress in shell-model studies, which have resulted in remarkable gains in our understanding of the structure of the nucleus. New effective nucleon-nucleon interactions have been constructed that contain both two- and three-body contributions. Information on the single-particle energies and two-body residual interactions can be derived from the experimental observables, such as single-particle energies, reduced transition probabilities and quadrupole moments [1], and it can be used to estimate the nuclear structure of more complex configurations. Thus, experimental data are needed in order to make robust predictions.

Transition probabilities, especially $B(E2)$ values, give particularly valuable insights into the nature of nuclear collectivity and its evolution with respect to the neutron (N) and proton (Z) numbers. For almost all the even-even nuclei, while augmenting the number of valence nucleons from the shell closure, the reduced transition probability $B(E2; 2^+ \rightarrow 0^+)$ increases progressively until a maximum value is reached around the mid-shell, where the number of degrees of freedom is maximum. The transition probability generally follows a parabolic trend across a major shell and it scales with the $B(E2; 2^+ \rightarrow 0^+)$ for the higher spin transitions [2]. In the regions near closed shells, as is the case in this paper, the seniority ν might be a good quantum number and it is defined as the number of unpaired particles in a state of angular momentum J. In this specific case, for the transitions conserving the seniority the $B(E2)$ values are maximum at the shell closures and reach the minimum in the mid-shell, exactly the opposite of the

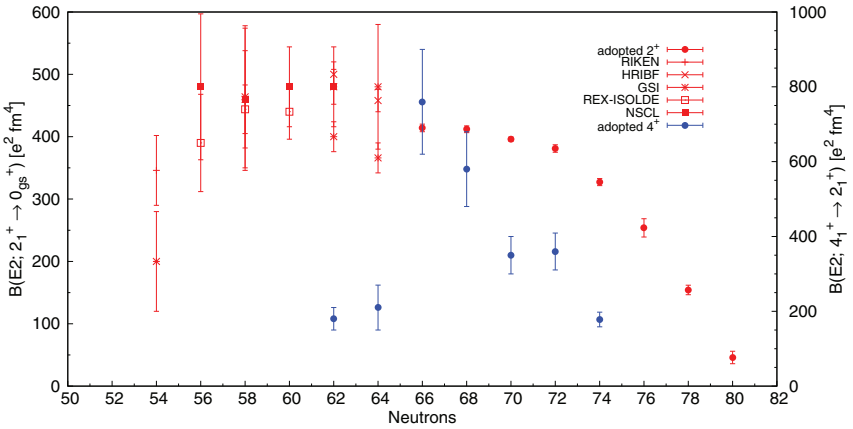

Fig. 1. – Systematics of the reduced transition probability (red) $B(E2; 2_1^+ \rightarrow 0^+)$ and (blue) $B(E2; 4_1^+ \rightarrow 2_1^+)$ for the Sn isotopic chain. For neutron-deficient Sn isotopes all the experimental values from previous experiments are reported. Data taken from [3].

$2^+ \rightarrow 0^+$ transition described before for which there is a change of seniority ($\Delta\nu = 2$). This change is due to the fact that in singly-magic even-even nuclei with more than two particles in a single shell for most residual interactions the $J > 0$ states will still be dominated by the breaking of a single pair, while 0^+ ground state must have the two particles coupled to spin zero. The deviation from this parabolic behaviour of the reduced transition probability could be a fingerprint of the creation/disappearing of a shell closure or of the presence of other phenomena, such as shape coexistence.

Thus, the structure of nuclei with few nucleons outside the double-shell closure $Z = N = 50$ has attracted large interest in the last years. Several studies were performed in this region to examine the robustness of the proton shell closure when $N = 50$ is approached. Because of the presence of low-lying isomers, the reduced transition probabilities in this neutron-deficient region were mainly determined via Coulomb excitation reactions [3, 4]. Along the whole isotopic chain the excitation energy of the first 2^+ and 4^+ states is well known and the behaviour is rather constant [5]. In fig. 1 for the neutron-rich Sn isotopes the reduced transition probability seems to follow the parabolic behavior with the maximum at the mid shell, which is the typical trend that one would expect for one-body even operator, such as the $B(E2)$. However, the information on the $B(E2; 2^+ \rightarrow 0^+)$ values for the neutron-deficient Sn isotopes suffer from large experimental uncertainties. Moreover there is a lack of information on the $B(E2; 4^+ \rightarrow 2^+)$, while their values would help to make a more robust physical interpretation.

The experiment described in this manuscript was devoted to the measurement of the reduced transition probability for ^{106,108}Sn by using the Recoil Distance Doppler-Shift (RDDS) method [6, 7] that provides a direct measurement of the lifetimes. This is a complementary method to the Coulomb excitation experiments performed up to date in this region. The nuclei of interest were populated via a multi-nucleon transfer reaction. Combining this reaction mechanism with a large angular acceptance magnetic spectrometer, a clear channel selection in both mass (A) and atomic number (Z) was obtained and it also allowed to control the feeding from higher-lying states via a gate on the Total Kinetic Energy Loss (TKEL) [6].

2. – Experiment

It was shown by Broda and collaborators [8] that neutron-deficient nuclei close to the $N = Z = 50$ region can be populated via multi-nucleon transfer reactions. The beam-target combination was optimized for the present lifetime measurement by choosing a cadmium beam and a molybdenum target, that will yield the beast rates for the nuclei of interest and will allow a good identification of the produced nuclei.

A ^{106}Cd beam, provided by one separated-sector cyclotron of the GANIL facility (France) at the energy of 770 MeV, impinged onto a 0.715 mg/cm^2 thick ^{92}Mo target. For lifetime measurements the RDDS method was employed using the differential Cologne plunger, placing a 1.6 mg/cm^2 thick ^{24}Mg degrader after the target. The degrader thickness and material were chosen in order to reduce the recoil velocity by $\Delta\beta \approx 1\%$ and also to minimize the parasitic counting rate due to the reaction of the beam with the degrader. In order to measure the lifetimes of interest 8 different target-degrader distances were spaced in the range 10–500 μm.

The complete A and Z identification, together with the velocity vector for the projectile-like products were obtained on an event-by-event basis using the VAMOS++ spectrometer [9-11], placed at the grazing angle $\theta_{lab} = 25^\circ$. In coincidence with the magnetic spectrometer the γ rays were detected by 8 AGATA Triple Clusters [12], placed at backward angles in a compact configuration.

2˙1. *AGATA.* – AGATA represents the state-of-art in γ-ray detectors and consists in a shell of HPGe crystals, each of them segmented electrically into 36 parts. A full digital signal treatment allows to perform a pulse shape discrimination and then eventually tracking. In addition it allows to correct the presence of unstable segments and neutron damages [13], in order to achieve the best apparatus performances. While dead-segment correction restores the position identification inside the crystal, the neutron-damage correction improve significantly the energy resolution. For example detector 04B, whose energy resolution of the core was 4.26 keV at 1332 keV, the FWHM improved down to 3.42 keV thanks to the neutron-damage correction.

After these corrections, the Pulse-Shape Analysis (PSA) [14] can be performed, providing the γ-ray interaction points inside every single crystal. Then, with the Pulse-Shape Analysis information the path of the γ rays inside the AGATA array can be reconstructed by using a tracking algorithm, such as the Orsay Forward Tracking (OFT) [15] or the Mars Gamma Tracking (MGT) [16] algorithm. The characteristic features of γ-ray tracking are based on the most relevant interaction mechanisms:

- Low-energy γ ray has a short mean free path and interacts with matter via photoelectric absorption, transferring its energy to the electron into an isolated interaction point.

- γ rays with energy from a few hundred keV to some MeV are absorbed in the detector with a sequence of (a few) Compton scattering interactions and a final photoelectric effect. Such events are reconstructed using a figure of merit that quantifies how well the scattering angles determined form the position of the involved interaction points agree with the values obtained inserting the pertinent energies into the Compton scattering formula. The figure of merit is calculated for all permutations of the interaction points and the event is accepted if the merit of the best permutation is compatible with an empirically defined limit.

- Above the threshold energy of 1.022 MeV, pair production events become important. A strong signature of this mechanism is given by the fact that the first point of interaction collects the total γ-ray energy minus the mass needed to create the electron-positron pair, while the two annihilation photons generate their own clusters of interaction points in the vicinity of this site.

In this work the tracking was performed by using the OFT algorithm. The first step of the tracking algorithm is to group the interaction points, deduced by the PSA, into clusters in the (θ, ϕ) plane sorting them according to increasing θ in order to make the cluster searching easier. Points are group in clusters according to their relative angular distance, which is adapted depending on the multiplicity of interaction points. For each cluster and each permutation of the interaction points using the target position as the source of the γ ray, a figure of merit is calculated. In order to be further processed, single interaction points must be well isolated hits: in the OFT algorithm it was decided that the closest interaction point must be physically at least 4 cm away. If this is the case, the figure of merit of the cluster is computed: the algorithm estimates the probability for the incident photon to travel the distance in germanium from the source to the position of the interaction point and then to undergo a photoelectric interaction.

In the OFT algorithm three empirical parameters can be modified to optimize the tracking performances in agreement with the goal of the experiment.

- SigmaTheta: effective position resolution of the interaction point. It is used to assess the goodness of the comparison between the angles from the positions and the angles from the deposited energies, given a sequence of interaction points.
- MinProbSing: in addition to the position requirement mentioned before, the minimum probability for accepting single interaction clusters defines a threshold for the calculated figure of merit. This probability threshold has the effect of an energy threshold below that events are rejected as background.
- MinProbTrack: the acceptance level of multiple-interaction clusters is defined by the minimum probability threshold for the figure of merit.

The value of these three parameters was optimised in order to maximise at the same time both Peak-to-Total ratio (P/T) and the efficiency [17]. As result of the optimization, in fig. 2 the comparison between the AGATA efficiency measured with a ^{152}Eu source is shown with and without tracking. In the energy region of low-lying transitions of the Sn isotopes, the tracking increases the efficiency up to 30%. On the other hand, for energies lower than 200 keV the efficiency is dropping when applying the tracking: while rejecting bad events for improving P/T, also good ones are discarded because of the tracking parameters. Moreover, in order to reduce the X-rays coming mostly from the beam and the target, 5 mm Cu absorbers were placed in front of the detectors. Because of the presence of these absorbers, the efficiency rapidly drops for energies lower than 400 keV, as it is shown in the same figure. Thus, these three parameters have to be optimised according to the goal of the experiment, being a compromise in order to have the best performances in the γ-ray energy region of interest.

2˙2. *VAMOS*. – The complete identification of the projectile-like fragments is provided by the magnetic spectrometer VAMOS++. At the entrance of the spectrometer the dual position-sensitive Multi-Wire Proportional Counter [11] measures the direction of the

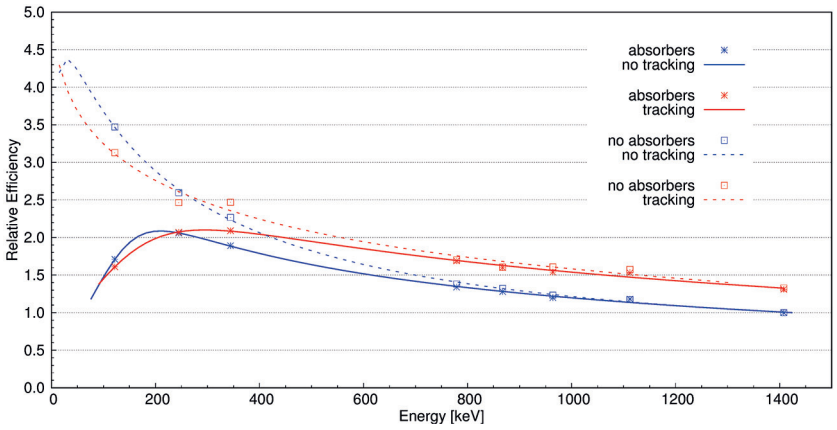

Fig. 2. – AGATA relative efficiency as function of γ-ray energy without (blue) and with (red) tracking, measured with ^{152}Eu. In order to reduce the X-rays coming mostly from the beam and the target, 5 mm Cu absorbers were placed in front of the detectors. The comparison between the relative efficiency without (squares) and with (stars) the absorbers shows the decrease at energies below 400 keV. The efficiency curve without the tracking has been normalised to 1 for the 1408 keV transition energy.

recoils, that is essential for defining the ions velocity vector. This detector together with a Multi-Wire Parallel-Plate Avalanche Counter placed at the focal plane [10] measures the time of flight of the fragments. The trajectories are reconstructed event by event via the transfer-matrix method with the information about the ion focal plane position and direction, which are provided by two Drift Chambers (DC). Just after the DC an segmented Ionization Chamber (IC) is placed to allows the Z identification. From the relativistic Lorentz-force formula, by knowing the ion velocity and the magnetic rigidity, it is possible to first separate the recoils according to the ratio between their mass and charge state. Then, considering in first approximation that the total energy deposited in the different sections of the IC is equal to the kinetic energy of the ion, it is possible to obtain the charge state of the recoils. Finally by combining the kinematic information with the charge state, the ion mass can be obtained.

3. – Results

By combining the information of the first interaction point in the AGATA detectors, provided by the γ-ray tracking algorithm, with the recoil velocity vector measured by VAMOS++, the Doppler correction of the emitted γ rays can be performed event by event. As it is shown in fig. 3, because of the energy loss inside the degrader the ion velocity decreases from β_S down to β_U which is directly measured by the magnetic spectrometer. The energy of the γ rays emitted after the degrader would be properly Doppler corrected, while the energy would be shifted at lower values for those emitted between the target and the degrader. The Doppler correction was optimised by correcting the recoil velocity ($\beta_U \approx 11\%$) for the energy loss inside all the VAMOS++ gas detectors and also by estimating the effective target-AGATA distance. Then, by gating on the ^{60}Ni, produced via the fusion-fission reaction of ^{106}Cd and ^{24}Mg, the quality of the Doppler correction can be checked and compared to the resolution obtained with ^{60}Co source.

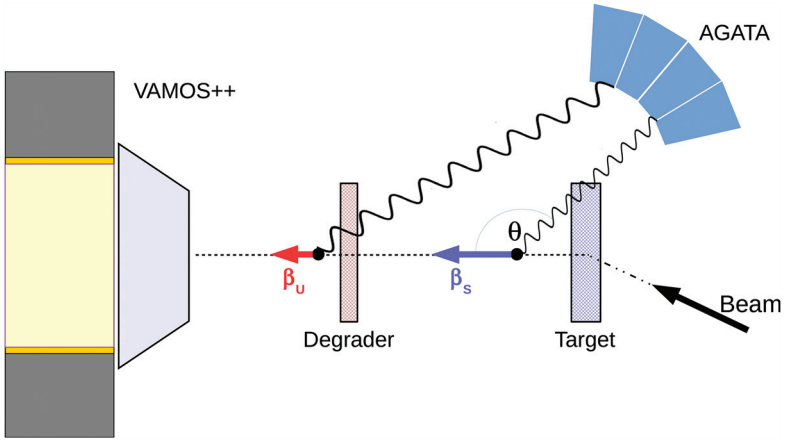

Fig. 3. – Recoil Distance Doppler-Shift method: after the reaction the fragment loses energy inside the degrader, whose material and thickness were chosen in order to decrease the ion velocity β_S by 1% of the speed of light. The velocity after the degrader β_U is directly measured by VAMOS++ and it is used for the Doppler correction. The energy of the γ rays emitted after the degrader would be properly corrected, while the γ-ray energy for those emitted between the target and the degrader will be shifted at lower values.

After the optimisation, the FWHM at 1332 keV was 5.3 keV. Thanks to the unique capabilities of AGATA and VAMOS++, it was possible to obtain an in-beam energy resolution just $\approx 30\%$ higher than what had been obtained with radioactive sources, that is quite remarkable considering the large velocity of the fragments. A good energy resolution is crucial for clearly separating the two components of each γ-ray transition when using the RDDS method. Example of this remarkable result can be found in [18].

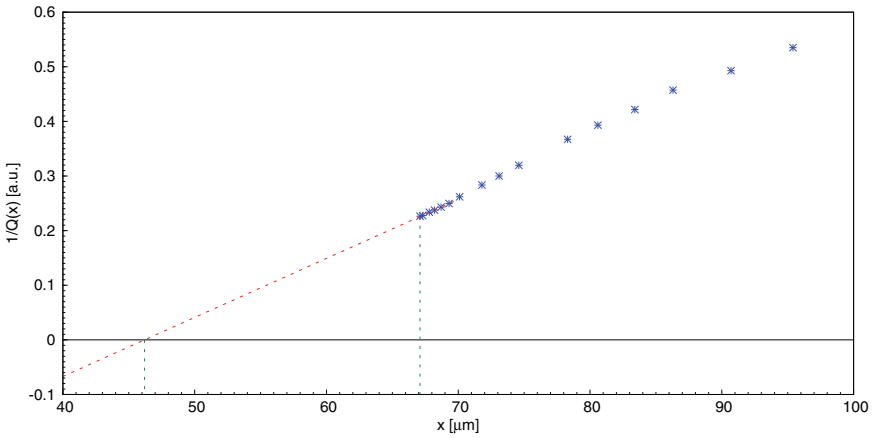

Fig. 4. – Inverse of the induced charge as a function of the distance between the target and degrader foils. For small target-degrader separation the trend is linear, so the position of the contact point ($1/Q(x) = 0$) can be extrapolated with a linear fit (red line). The plunger zero offset is represented by the difference between the extrapolated and the measured contact point positions (green line).

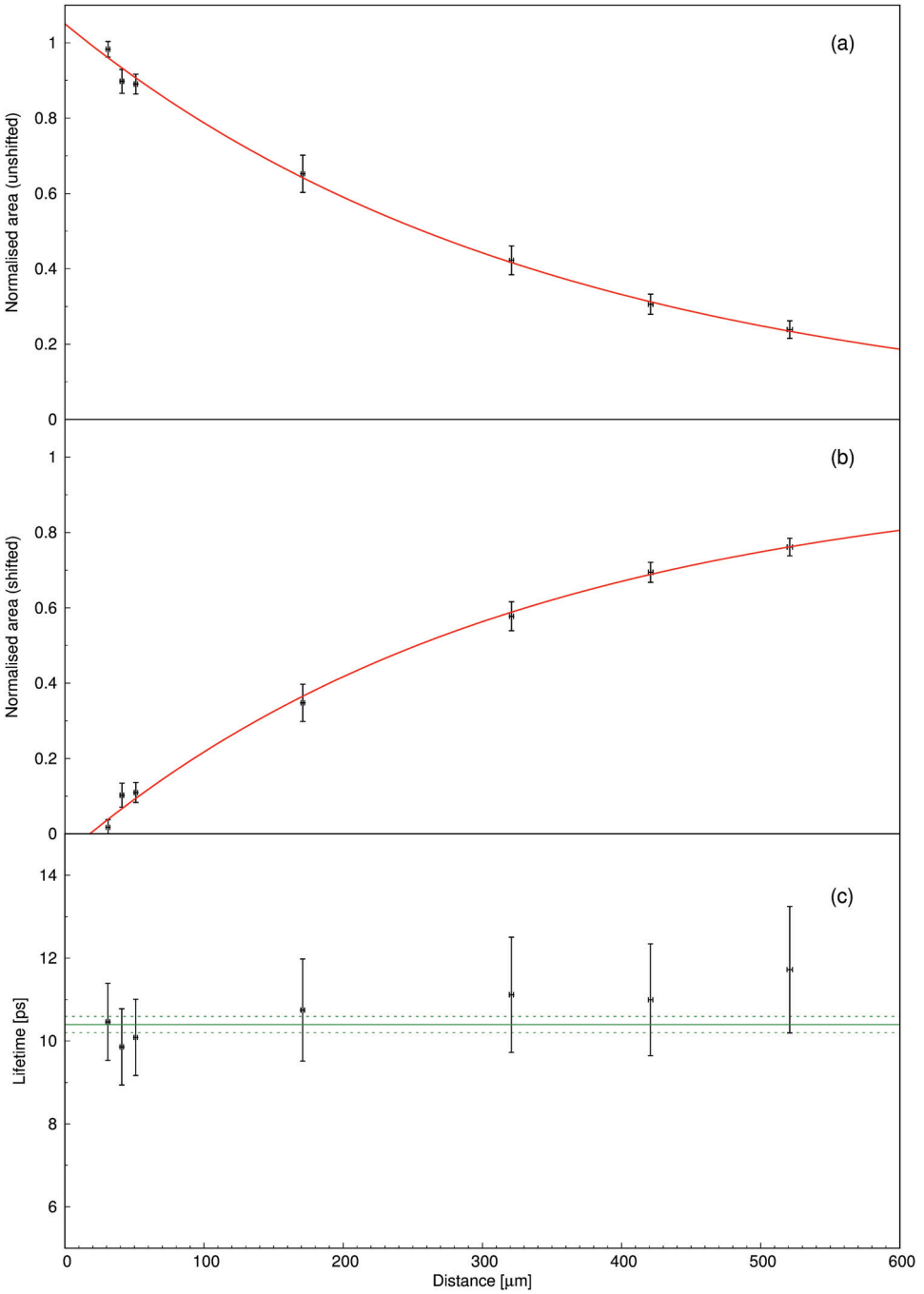

Fig. 5. – Lifetime measurement of the first 2^+ state of ^{106}Cd via DCM and DDCM: (a) "unshifted" and (b) "shifted" area, normalized over their sum, (c) DDCM lifetime results as a function of the proper target-degrader distance. The solid line represents the fitting function, while the green dashed ones are the lifetime result error bars.

TABLE I. – *Comparison between the lifetimes obtained via Decay-Curve Method, Differential Decay-Curve Method and the value from literature* [21]. *The DDCM measurement is the weighted average of the results reported in fig. 5(c).*

DCM	DDCM	Literature
10.7(4) ps	10.4(2) ps	10.5(1) ps

For lifetime measurement via Decay-Curve Method (DCM) the absolute target-degrader distance is necessary, while the plunger gives information on the degrader position with respect to an internal reference. Thus, after optimizing the Doppler correction, the evaluation of the plunger zero offset has been checked in order to obtain the absolute distances. The minimal target-degrader distance was determined with the capacitance method [19]: while decreasing the foils separation down to the contact point and sending a pulsed signal through the plunger, the induced charged is measured. In the case of two planar foils with area A, the induced charge $Q(x)$ as a function of the distance x goes as the inverse of the separation between the foils, as it is described as follows:

$$Q(x) = C(x)V = \epsilon_0 \epsilon_r \frac{A}{x} V, \tag{1}$$

where ϵ_0 and ϵ_r are the dielectric constant in vacuum and the relative dielectric constant, respectively. This asymptotic trend is real for small target-degrader distance. Thus, by plotting the inverse of the induced charge as function of the plunger distance, it is possible to estimate the position of the contact point ($1/Q(x) = 0$), as it is shown in fig. 4. From the difference between the estimated contact point and the measured one, the plunger zero offset can be obtained and the found value was 20.9 ± 1.2 μm.

The lifetime, calculated via DCM with the estimated offset, was compared with the one extracted via the Differential Decay-Curve Method (DDCM) [8, 20], that depends just on the relative distance between two points. In fig. 5(a) the decay curve for the first 2^+ state of ^{106}Cd is presented, after gating on the fast component of the feeding transition coming from the first 4^+ state. Then fig. 5(b) shows a fitting function in order to obtain its derivative, that is necessary for the lifetime determination via DDCM. The results obtained with this second method are finally reported in fig. 5(c). The lifetime of the first 2^+ state of ^{106}Cd has been measured with these two different methods, by gating on the shifted component of the first 4^+ state in order not to account for the feeding from higher excitation energy states. The result obtained via DCM is in agreement with the lifetime obtained with the DDCM and both are in agreement with the known value in literature [21]. These preliminary results are summarized in table I.

4. – Conclusions

The neutron-deficient region close to $N = Z = 50$ shell closure has been successfully populated via the multi-nucleon transfer reaction ^{106}Cd+^{92}Mo. The AGATA array, coupled to the magnetic spectrometer VAMOS++, provided a clear selection of the channel of interest in coincidence with the emitted γ rays. Thanks to the good position sensitivity of the VAMOS++ spectrometer and the excellent tracking performances of AGATA, an excellent in-beam γ-ray energy resolution of 0.4% at 1332 keV has been

obtained. The plunger device was used to determine the lifetimes of the excited states in this region. In order to check the validity of the setup, the lifetime of the first 2^+ excited state in ^{106}Cd has been measured via two different methods, DCM and DDCM. The preliminary results are in perfect agreement with the value reported in the literature. Further work is necessary for the lifetime determinations of the excited states of the $^{106-108}$Sn and the nuclei in the region.

* * *

The author would like to thank all the participant to this experiment as well as the AGATA and VAMOS communities. Special thanks go to the IKP group for the plunger and to the GANIL technical staff for their help in setting up the setup and the good quality beam. This work was partially supported by European Union's Horizon 2020 research and innovation programme (ENSAR, experiment E664), the Scientific and Technological Council of Turkey (TUBITAK, Proj. no. 114F473) and the Ministerio de Economia y Competitividad of Spain (EEBB-I-15-09671).

REFERENCES

[1] Maier K. H. *et al.*, *Eur. Phys. J. A*, **14** (2002) 349.
[2] Ressler J. J. *et al.*, *Phys. Rev. C*, **69** (2004) 034317.
[3] Doornenbal P. *et al.*, *Phys. Rev. C*, **90** (2014) 061302.
[4] Bader V. M. *et al.*, *Phys. Rev. C*, **88** (2013) 051301.
[5] Kumar R. *et al.*, *Phys. Rev. C*, **81** (2010) 024306.
[6] Valiente-Dobón J. J. *et al.*, *Phys. Rev. Lett.*, **102** (2009) 242502.
[7] Dewald A. *et al.*, *Prog. Part. Nucl. Phys.*, **67** (2012) 786.
[8] Broda R., *J. Phys. G: Nucl. Part. Phys.*, **32** (2006) R151.
[9] Pullanhiotan S. *et al.*, *Nucl. Instrum. Methods A*, **593** (2008) 343.
[10] Rejmund M. *et al.*, *Nucl. Instrum. Methods A*, **646** (2011) 184.
[11] Vandebrouck M. *et al.*, *Nucl. Instrum. Methods A*, **812** (2016) 112.
[12] Akkoyun S. *et al.*, *Nucl. Instrum. Methods A*, **668** (2012) 26.
[13] Bruyneel B. *et al.*, *Eur. Phys. J. A*, **49** (2013) 61.
[14] Söderström P. A. *et al.*, *Nucl. Instrum. Methods A*, **638** (2011) 96.
[15] Lopez-Martens A. *et al.*, *Nucl. Instrum. Methods A*, **533** (2004) 454.
[16] Bazzacco D., *Nucl. Phys. A*, **746** (2004) 248.
[17] Siciliano M. *et al.*, *LNL-Annual Report*, **250** (2017) 102.
[18] Siciliano M. *et al.*, *Acta Phys. Pol. B*, **48** (2017) 331.
[19] Alexander T. K. and Bell A., *Nucl. Instrum. Methods*, **81** (1970) 22.
[20] Dewald A. *et al.*, *Z. Phys. A At. Nucl.*, **334** (1989) 163.
[21] Kumbartzki G. J. *et al.*, *Phys. Rev. C*, **93** (2016) 044316.